International Journal of Pressure Vessels and Piping 199 (2022) 104775

Contents lists available at ScienceDirect

International Journal of Pressure Vessels and Piping

journal homepage: www.elsevier.com/locate/ijpvp

Stress Concentration Factor in vessels with circular crosshole: Continuous parameters analysis

Jaime Gimeno [a], Oscar Venegas [b,*], Javier Urbano [b]

[a] Polytechnic University of Valencia, Valencia, Spain
[b] Colombian School of Engineering Julio Garavito, Bogotá, Colombia

ARTICLE INFO

Keywords:
Stress concentration factor
Thick pressure vessels
Crossholes
High-pressure vessels
Finite element method

ABSTRACT

In this paper, a parametric study of the Stress Concentration Factor (*SCF*) has been carried out in cylindrical pressure vessels with circular holes. A three-dimensional finite element analysis has been carried out performing a variation of dimensionless parameters (thickness ratio, size ratio and aspect ratio) exploring a wider range than other investigations. It is observed that the maximum value of the *SCF* increases as the hole size ratio and the aspect ratio increase, although the location of the maximum *SCF* is located from the internal area of the vessel to the external part depending on the geometric configuration, defining thus three differentiated zones. Additionally, in the final part of the document, a fit model is defined to determine the value of the maximum *SCF* for different continuous values of the defined dimensionless parameters. This model allows to quickly calculate or locate from a contour map the maximum value of *SCF* for a specific geometry of pressure vessel.

1. Introduction

Pressurized vessels (tanks and pressurized fluid pipelines) have various applications both in industrial processes and research, and holes are commonly found in their walls to connect with other elements or accessories related to the process to be developed, to measure some variable or simply as sight window [13,16,18,22]. The presence of these holes in the pressure vessels, acts as a stress concentrator, increasing significantly the local stress than those present at normal section of the vessel, without any concentrator. The stress concentration depends mainly on the geometric characteristics of the vessel, the hole, its position, alignment and inclination [19].

An important indicator is the Stress Concentration Factor (*SCF*), which relates the maximum stress near of hole in the vessel, with the maximum stress of the same container without hole. This indicator is often used in the pressurized cylindrical vessels design to preliminarily estimate the stresses to which the vessel is subjected and thus determine different additional variables such as size, thickness, geometry and indirectly make a budget of the project.

The aim of this paper is to study the behavior of *SCF* in cylindrical pressure vessels with circular holes through its wall, with the thickness ratio, the aspect ratio or slenderness and the size ratio of the hole with respect to the internal diameter of the cylinder as variables. To get a global understanding of *SCF* behavior, the parametric variation range of the considered variables is wider than what explored in other studies [2,14,15,17,23], and the location of maximum stress and *SCF* maximum values due the hole have been determined using a Finite Element Analysis (FEA) software. In addition, a useful fit model is proposed to easily find the value of the Stress Concentration Factor for a specific geometric configuration.

This document is structured in six sections. Section 2 shows the state of the art related to behavior of *SCF* pressure vessels with holes. In section 3, the parameters and operating conditions established for the simulations are disclosed, as well as the identification of the points of interest where the maximum *SCF* is presented. Subsequently, section 4 presents the results and its discussion, including *SCF* value and location analysis respect to variations of geometric parameters and the contrast with the data found by other authors.

In section 5, a correlation from the continuous analysis of the three geometric relationships previously established in the study (thickness ratio, aspect ratio and hole size ratio) is proposed, in order to mathematically predict the value of the *SCF* for any geometry that can be used in a cylindrical pressure vessel. Finally, section 6 presents the main conclusions of the study and possible future work.

* Corresponding author.
E-mail addresses: jaigigar@mot.upv.es (J. Gimeno), oscar.venegas@escuelaing.edu.co (O. Venegas), javier.urbano@escuelaing.edu.co (J. Urbano).

https://doi.org/10.1016/j.ijpvp.2022.104775
Received 13 July 2022; Accepted 8 August 2022
Available online 13 August 2022

2. Theoretical background

Geometric variables related to this type of concentrators are mainly derived from the geometry of the vessel and the holes they have. According to Fig. 1, the following geometric variables are defined in a closed end cylindrical vessel with a crosshole: main cylinder length (L), outer radius of the cylinder (R_e), inner radius of the cylinder (R_i) and hole radius (R_a).

The relationships between these geometric variables define dimensionless parameters that lends to compare to related investigations [4,11,20]. These dimensionless relationships are defined as: thickness ratio (R_e/R_i) obtained from relating the external and internal radius of the cylinder, aspect ratio or slenderness calculated from the ratio between cylinder length and the outer diameter ($L/(2R_e)$), and the size ratio of the hole derived from the ratio between the radius of the hole and the inner radius (R_a/R_i).

Other authors have used similar parameters, with some variations in their definitions and values [11,19]. Specifically, aspect ratio or slenderness values are defined based on specific investigation objectives, and their definition is different and in some cases are not clearly indicated. Makulsawatudom et al. [14] and Camilleri et al. [2] used a ratio of $L/(2R_e) = 1$; Dixon et al. [4] used the Decay cylinder length concept, Masu [15] used $L/(2R_e) \geq 2$; Kharat [9] used a ratio $L/(2R_e) = 3$; Iwadate et al. [8] used a $L/(2R_e)$ ratio between 2.7 and 3.2; Raju [23] used a ratio $L/(2R_e) = 1.2$; and finally Kihiu et al. [12], Adenya [1] and Nihous [19] used a L value of nine times the wall thickness. The ranges of the parameters considered by the cited authors are summarized in Fig. 2.

In any case, the *SCF* calculated by several authors retains the concept of relating the maximum stress of the vessel with hole and the maximum stress of the same vessel without hole. The maximum tangential stress on a cylinder without a hole is calculated with equation (1) proposed by Lamé [24], where R_e and R_i, are respectively the external and internal radius of the vessel and p is the internal pressure of the vessel. Lamé equations assume a homogeneous and isotropic material with linear elastic deformations.

$$HoopStress = \sigma_{Hoop} = p\left[\frac{(R_e/R_i)^2+1}{(R_e/R_i)^2-1}\right] \tag{1}$$

In closed ends cylindrical vessels without crosshole, the tangential stress (σ_θ) or Hoop Stress (σ_{Hoop}), are equal to the maximum main stress (σ_{1max}). However, to perform the calculation of the *SCF* in pressure

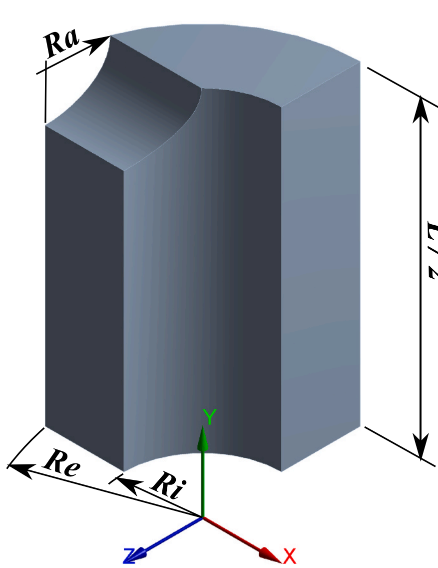

Fig. 1. Reference geometry and nomenclature in cylindrical vessels.

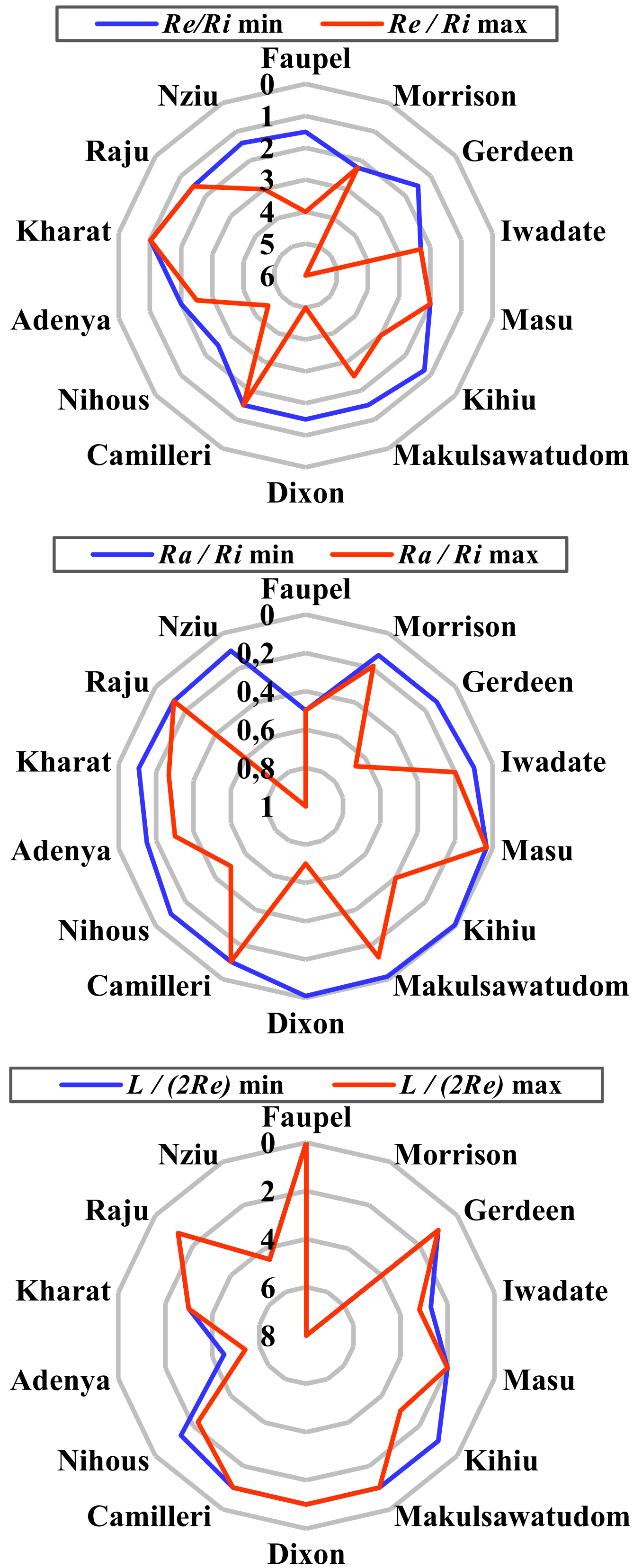

Fig. 2. Ranges of values for the parameters analyzed by different authors.

vessels with crosshole, different relations are used according to the specific aim of the study and there is not consensus among the authors. The maximum stresses and their respective *SCF* are indicated as: the maximum tangential or hoop stress ($\sigma_{\theta max}$) and $SCF_{\theta max}$ (equation (2)), the maximum main stress (σ_{1max}) and SCF_{1max} (equation (3)), the maximum shear stress (τ_{max}) and $SCF_{\tau max}$ (equation (4)), and the maximum equivalent or maximum von Mises stress (σ_{emax}) and $SCF_{\sigma emax}$ (equation (5)), where σ_{ec}, is the value of the equivalent stress of plain cylinder calculated from the Lamé solution [3].

$$SCF_{\theta max} = \frac{\sigma_{\theta max}}{\sigma_{Hoop}} \tag{2}$$

$$SCF_{1max} = \frac{\sigma_{1max}}{\sigma_{Hoop}} \tag{3}$$

$$SCF_{\tau max} = \frac{2\tau_{max}}{\sigma_{Hoop}} \tag{4}$$

$$SCF_{\sigma emax} = \frac{\sigma_{emax}}{\sigma_{ec}} \tag{5}$$

Table 1 presents a summary of types of *SCF* estimated by each author using equations (2)–(5) and the methodology employed. The *SCF* values found by each author vary depending on the relationships established, and the way in which the study was conducted, either analytically, by finite element models or experimental test.

The following sections present a global study, using wider ranges of geometric relations, allows comparison with other results found in the literature. This approach, also enable to learn more about the trend in location and value of the maximum *SCF* in cylindrical vessels with holes.

3. Simulation setup and validation

This simulation apply for cylindrical vessels with closed ends, centered crosshole, and with internal pressure applied on main vessel surface and crosshole surface. In this study, it is considered a thick-walled cylinder with closed ends and a crosshole whose geometric variables, R_a, R_e, R_i and L, as shown in Fig. 1, related to each other to obtain dimensionless parameters that can be subsequently compared to the results obtained by other authors. For the cylinder with crosshole centered on both, length and diameter, 1008 models were considered taking different values of geometric relations, R_e/R_i, $L/(2R_e)$ and R_a/R_i as shown in Table 2. A fixed value of R_i was defined for all models, 100 mm, similar to the study conducted by Comlekci et al. [3]. Values lower than $R_e/R_i = 1.125$ were not considered since usually considered to correspond to the thin sheet theory which is beyond the scopes of this study. According to the range given in Table 2, the L values were between 84 mm and 1600 mm; R_e between 112 mm and 400 mm and R_a between 1.25 mm and 98.75 mm; considering that in the range of R_a/R_i between 0.9 and 0.9875 for values of $L/(2R_e)$ equal to 0.625, 0.75 and 0.875 are geometrically incompatible.

To study the effect of geometry on generated stresses for a cylindrical pressure vessel, the simulation was conducted using ANSYS Workbench, applying parametric functionality to vary cylinder and holes dimensional values to get the parameters values predefined and specific results (maximum principal stress and its 3D position). For all simulations, the modeling of 1/8 of a symmetrical cylinder was performed, with respect to three planes of symmetry (Fig. 3). First plane (face E) is perpendicular to the base F that passes through the center of the cylinder and the hole, the second plane (face D) perpendicular to face E and base F and passes through the center of the cylinder and the third plane (face C) parallel to base F and passes through the center of the hole. Fig. 3 (left side), shown an example of the geometry used for simulations.

An unstructured mesh using three dimensional tetrahedral solid elements, *10−node* isoparametric (Solid187 elements) was used in order to adapt mesh to huge number of models. Because the variation in stress values occurs mainly around the edges and corners near the hole, and according to the FEA results of Comlekci [3] and Nihous [19], a local refinement was included for the mesh. Fig. 3 (right side) shown the refinement detail. This refinement, similar to Nihous [19], leads sizing of the elements close to the selected edges achieving a balance between the processing time and the reliability of the data obtained in the area of interest, getting a precise identification of the position of the maximum principal stress in zones nearest or along the edges of the hole. Due to the dimensional difference of the models presented in Table 2, especially the length, reference mesh sizes were used, carrying out the respective mesh convergence for each model; thus obtaining, in general, seed elements from 5 mm and adapted according with total volume for each model.

Regarding the boundary conditions, a vessel with closed ends was assumed, then, base F was studied as completely rigid, while the faces D and E were considered deformable in the radial and longitudinal directions. In addition, a distributed load was applied to face C according to the load applied by the rigid closed ends, taking into account 1/4 of this load and the geometry for each simulation. The internal pressure of the cylinder for all simulated models was imposed at 17.5 MPa and this value was applied both to the internal surface of the cylinder (B) and to the surface of the hole (A). Because rigid face F assumption it not real, it can be derived in different results. Also, the faces on which the pressure

Table 2
Established values for the simulations.

Parameter	Values
R_e/R_i	1.125, 1.25, 1.5, 1.75, 2, 2.25, 2.5, 3, 4
R_a/R_i	0.0125, 0.025, 0.05, 0.075, 0.1, 0.2, 0.3, 0.4, 0.5, 0.6, 0.7, 0.8, 0.9, 0.95, 0.975, 0.9875
$L/(2R_e)$	0.625, 0.75, 0.875, 1, 1.5, 2, 3, 4

Table 1
Types of calculated stress and related methodology.

Autor	$\sigma_{\theta max}$	σ_{1max}	τ_{max}	σ_{emax}	FEM
Faupel [6] [a]	X				
Morrison [17] [a]	X		X		X
Gerdeen [7] [b]	X				
Iwadate [8] [a]	X				
Masu [15]		X			X
Kihiu [12]	X				X
Comlekci [3]		X		X	X
Dixon [5]		X	X		X
Camilleri [2]	X				X
Nihous [19]		X			X
Adenya [1]	X				X
Kharat [9] [a]	X				
Raju [23]	X			X	X
Nziu [20]	X				X

[a] Experimental method.
[b] Analytic method.

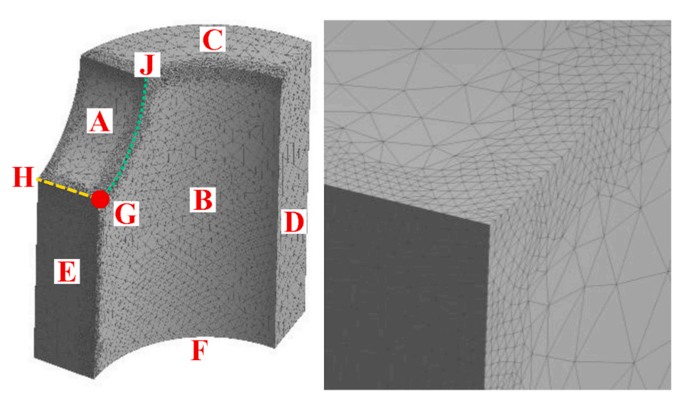

Fig. 3. Mesh of 1/8 cylinder. Left-General view, Right-Refinement in areas of interest.

is applied can also affect the numerical result. Some authors did not use pressure on face A and other studies do not provide information on pressure on this face. To analyze each model, a carbon steel material with a modulus of elasticity of 200 GPa, a Poisson's ratio of 0.3, a yield strength (S_y) of 250 MPa and an ultimate strength (S_u) of 400 MPa was used, applying a linear stress analysis. Table 3 summarizes main issues related to simulation.

In order to validate the parametrization of the mesh, simulations of vessels without hole ($R_a/R_i = 0$) are initially performed for all ranges of R_e/R_i and $L/(2R_e)$ shown in Table 2 and these results are compared with equation (1) proposed by Lamé. In Fig. 4, it is observed that the principal stress values for different thickness and aspect ratios are properly adjusted to the Lamé equation, finding a maximum average deviation of 8.5% for the thickness ratios R_e/R_i smaller and tending to decrease to one third at higher values of R_e/R_i, showing that the mesh parameterization used in the simulations is consistent with the Lamé equation. In general, it is observed that for aspect ratios $L/(2R_e)$ less than unity and for values of R_e/R_i close to 1, the deviations of the simulation with respect to the calculation with equation (1) increase. A final post process was performed to estimate the SCF_{1max} (equation (3)), from σ_{1max} obtained from simulations and σ_{Hoop} calculated from Lamé equation.

4. Results and discussion

In this section, the results obtained from the simulations are shown taking into account the different possible combinations of Table 2, where an elastic linear analysis was carried out, finding that in most of the cases analyzed (approximately 60%) the maximum *SCF* is located in the G corner of the hole (see Fig. 3 left side), which in agreement with various studies that define corner G as the most critical [14,20]. However, Nziu [20] highlights that for certain configurations of R_a/ R_i and R_e/R_i, the maximum stress was not found in the corner G of the hole but on the edge adjacent to the cylinder (edge G-J in Fig. 3 left side).

From the results obtained from the present study, it is observed that in thick-walled cylinders with very small holes, the location of the point of maximum stress moves from the corner G to the exterior of the cylinder (edge G-H in Fig. 3 left side), such as it is observed in Fig. 5 for a 75 mm thick wall thickness with a maximum stress located 1 mm from the corner G on the edge G-H. Fig. 6 shows a cylinder with the same values of R_a/R_i and $L/(2R_e)$ of the previous case but with a thicker wall, 200 mm, showing that the behavior is similar to that shown previously, moving along the edge G-H outwards.

On the other hand, when reviewing values of $R_e/R_i = 1.125$ and $L/(2R_e) = 1.5$ for different values of R_a/R_i; the displacement of the maximum point *SCF* is notable. In Fig. 7a, it is observed that for values of R_a/R_i close to 0.5 the point of maximum principal stress is located slightly away from the corner G on the edge G-J and as the ratio R_a/ R_i increases, the maximum *SCF* moves on the same edge (G-J) moving further away from the corner G (Fig. 7b), even reaching values close to $R_a/2$ (Fig. 7c). In other more critical cases, as R_a/R_i approaches 1, the point of maximum stress after moving away from G on edge G-J, also moves outwards, thus finding the maximum *SCF* covering part of face A

Table 3
Simulation conditions.

Information	*Description*
Software	ANSYS Workbench
Element	3Dsolid 10–node isoparametric, Solid187
Mesh	Unstructured Mesh. Refined in specific Edges
Symmetry	3 planes
Internal Pressure	17.5 MPa
Material	Carbon Steel Linear elastic
Analysis Type	Parametric Linear elastic
Geometric variables	R_e/R_i, R_a/R_i and $L/(2R_e)$
Output	Max Principal Stress and its 3D Location
Simulated models	1008

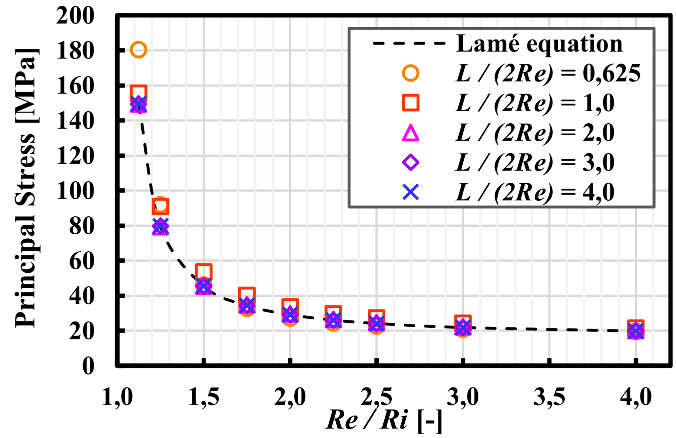

Fig. 4. Validation of mesh parameterization with Lamé's equation for cylinders without holes.

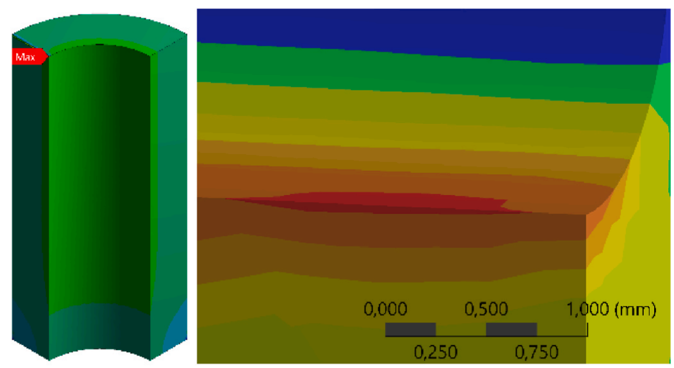

Fig. 5. Point of maximum stress for $R_a/R_i = 0.0125$; $R_e/R_i = 1.75$ and $L/(2R_e) = 3$. Left-General View and Right-Detail of the position of the maximum main stress point.

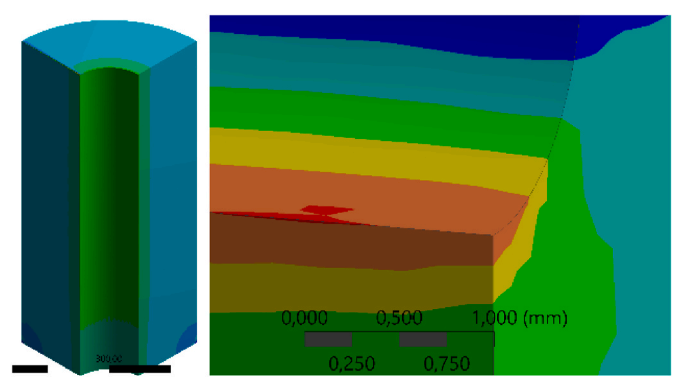

Fig. 6. Point of maximum stress for $R_a/R_i = 0.0125$; $R_e/R_i = 3$ and $L/(2R_e) = 3$. Left-General View and Right-Detail of the position of the maximum main stress point.

as seen in Fig. 7d and e. The above is an extreme case, close to the theory of a thin sheet for vessels (cylinder wall thickness is less than 10% of the cylinder radius [24]), which makes it difficult to propose an analytical theory, due to the change in position point of maximum stress. Finally, for values of $L/(2R_e)$ less than unity, the behavior is similar to that shown in Fig. 7d and e; i. e, the maximum *SCF* is presented on face A.

Fig. 8 represents the location of the maximum *SCF* presenting the percentage of the radius of the hole R_a on the abscissa (X axis), showing how far the maximum *SCF* is from corner G along edge G-J, and on the

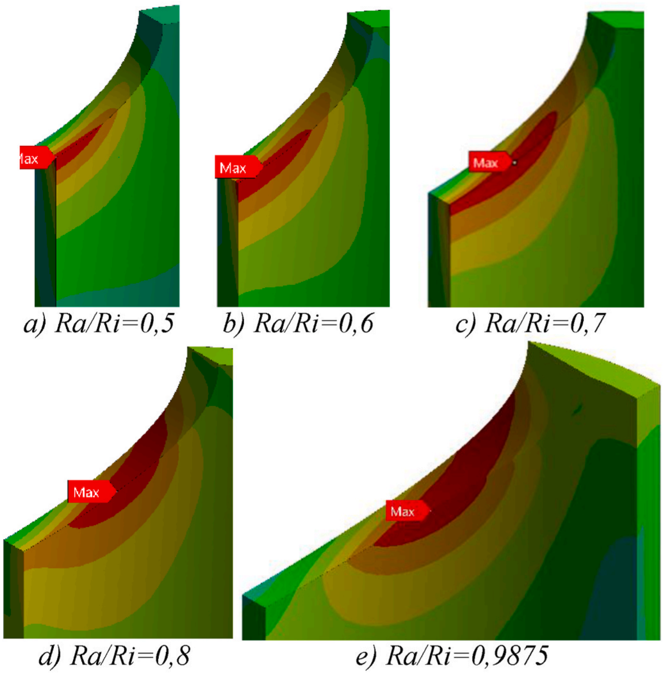

Fig. 7. Point of maximum stress for $R_e/R_i = 1.125$ and $L/\ (2R_e) =\ 1.5$.

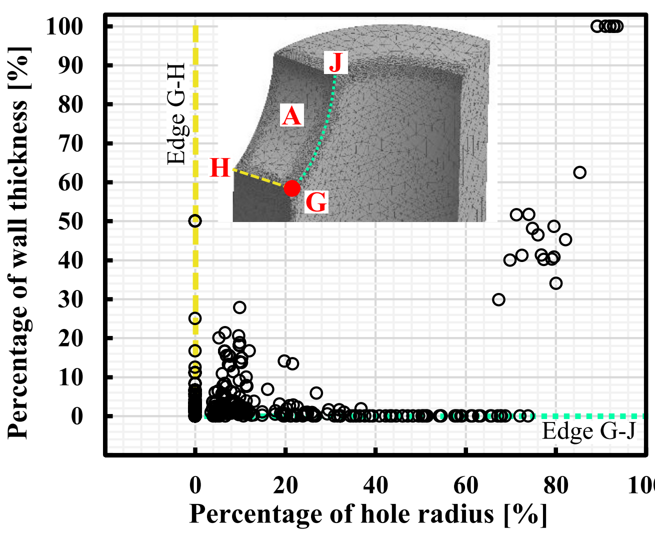

Fig. 8. Location of the maximum *SCF* for all the values studied.

ordinate (Y axis) the percentage of wall thickness, showing how far the maximum *SCF* is from the corner G by the normalized edge G-H with respect to the thickness of the cylinder. Fig. 8 shows that most of the cases are in the area near the corner G, especially on the edge G-J, edge G-H and on the surface A. The other points are seen on the surface A and in some of the simulated cases, the point of maximum *SCF* extends to outer cylinder wall (100% wall thickness).

In order to deepen and link the location of the points in Fig. 8 with the thickness ratio (R_e/R_i) and the hole size ratio ($R_a/\ R_i$) for all aspect ratio ranges ($L/(2R_e)$) studied, in Fig. 9 different zones are shown depending on these relationships.

It is possible to see that for all the cases of $R_a/R_i\ = 0.3$, independent of the other variables, the point of maximum *SCF* is located in the corner G, which coincides with the studies of Nziu [21]. Thus, Fig. 9 is divided into three zones, depending on the possible combinations with the other geometric relationships throughout its range. A first zone named Z1 for combinations with values of $R_a/R_i > 0.3$; a second zone called Z2 for combinations with $R_a/R_i\ = 0.3$, and a third zone called Z3 for combinations with $R_a/R_i < 0.3$.

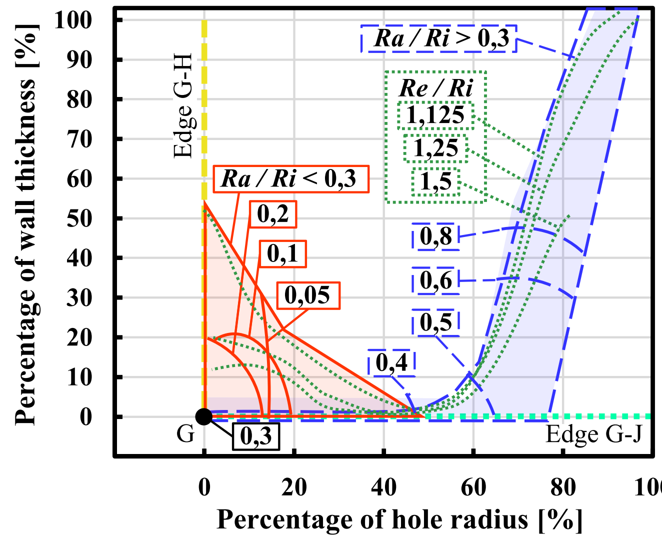

Fig. 9. Maximum *SCF* location zones.

Zone Z1, is delimited by the blue dotted line, corresponding to values of $R_a/R_i > 0.3$ and where the points of maximum *SCF* move moving away from point G on edge G-J as R_a/R_i increases until it reaches a value close to 0.5, where the distance is approximately 70% of the hole radius, and then moving away towards the center of surface A for values of $R_a/R_i > 0.5$ reaching in some cases up to the outer wall of the cylinder. The Z3 zone delimited by the solid red line corresponds to values of $R_a/R_i < 0.3$, where the maximum point *SCF* is not located beyond 40% of the hole radius and all the values of this zone come off the surface internal up to a maximum of 50% of the wall thickness. As the values of R_a/R_i approach zero, the values have more dispersion in the delimited zone; which may be an effect of the size of the hole in the model and it is consistent with most of the Nziu data [21].

The zones previously described show the limit zones of the values of R_a/R_i. It is also possible to see that for the same value of R_a/R_i, the limits for the values of R_e/R_i close to 1.25 tend to be further away from the internal surface of the cylinder, while those values closer to 3.0 are closer to both the inner surface and the corner G. Fig. 10 clearly shows this last variation for R_e/R_i in the area near the corner G. The variations

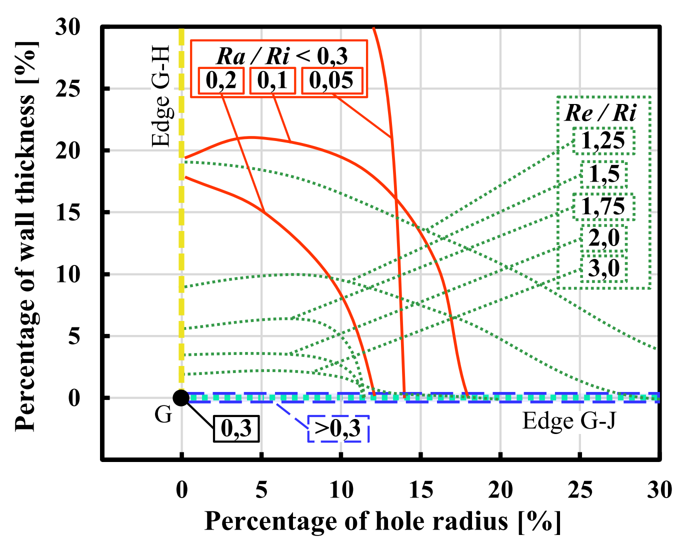

Fig. 10. Detail of the location zones of the maximum *SCF*.

of $L/(2R_e)$ distribute the data in the areas delimited by the other two variables, making the locations move towards or away from the G corner.

The detail of the position in zones close to the corner G (Fig. 10), can be very useful for designers of this type of vessels, since it allows easy positioning the maximum *SCF* or at least know the tendency that these may present in failure analysis investigations with similar geometric relationships.

Fig. 11 shows the location of these maximum points as a function of the combinations of R_a/R_i, R_e/R_i and $L/(2R_e)$ and the zones described above, which are delimited by envelopes with iso-values of $L/\ (2R_e)$. In Fig. 11 the values of $L/(2R_e) = 2$ are shown, since it is a value widely used in this type of study and the directions to where these enveloping limits move are indicated with arrows.

Analyzing Fig. 11, when using combinations of values of $R_a/\ R_i > 0.3$ and $R_e/R_i > 1.75$ the position will always be in the corner G (zone Z2). For combinations of values of $R_a/R_i > 0.3$ and $R_e/R_i < 1.75$ and depending on the envelopes $L/(2R_e)$, the maximum point *SCF* will be located in zone Z2 or in the zone Z1. For combinations of values of $R_a/R_i < 0.3$ and $R_e/R_i > 1.5$, it depends on the value of $L/\ (2R_e)$; thus, for values of $L/(2R_e)$ close to the lower limit of the study, 0.75, the point of maximum *SCF* is in the corner G; as the values of the envelopes $L/\ (2R_e)$ increase, the probability that the maximum point *SCF* is in zone Z2 increases, too.

The results shown in zone Z3 of the present study coincide with the results of Masu [15], Makulsawatudom [14], Kihiu [10] and Adenya [1]. Also, the results of the present study are consistent with the data of Nziu y Masu [21] (shown as circles in Fig. 11), which provide more information on the positions of the maximum *SCF*.

Fig. 12 shows a comparison between some values of $R_e/\ R_i$ for $L/(2R_e) = 2$ with the data of various authors who evaluated cylinders with through holes such as Masu [15], Dixon [4], Nihous [19] and Nziu [20], finding average percentage deviations lower than 6% and with a standard deviation of 0.084.

Finally, in Fig. 13, the maximum *SCF* data for all ranges of the dimensionless parameters studied in this document are exposed, showing that for each value of $L/(2R_e)$ the *SCF* increases as parameter R_e/R_i gets smaller for values of R_a/R_i between 0.2 and 0.4; for values of R_a/R_i less than 0.1 the *SCF* increases as the parameter $R_e/\ R_i$ is larger and lastly, values of R_a/R_i greater than 0.4 do not follow the same trend for small values of R_e/R_i (1.125, 1.25 and 1.5). 9.1 was the highest *SCF* value found (for $R_e/R_i = 1.25$; $L/(2R_e) = 4$; $R_a/R_i = 0.9875$) and the

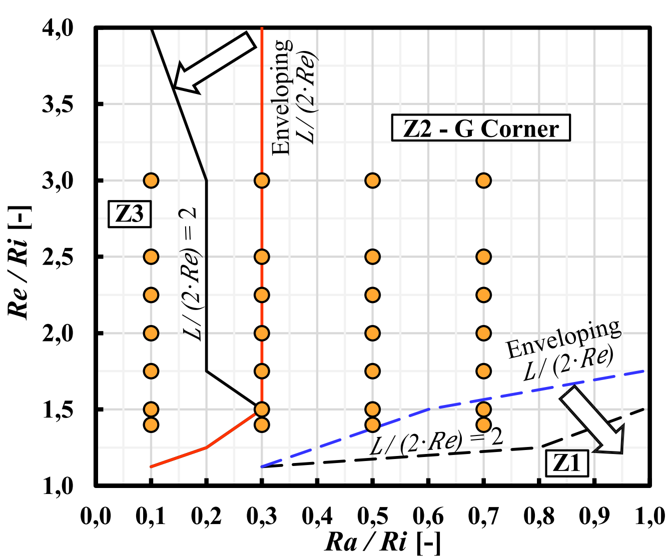

Fig. 11. Location of maximum point of *SCF* and comparison with data from Nziu and Masu [18] (circles).

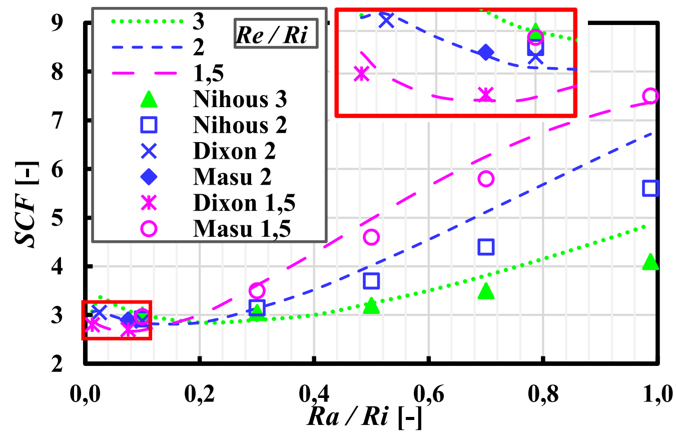

Fig. 12. Comparison of *SCF* from simulations (lines) with other authors for $L/(2R_e) = 2$ and different values of R_e/R_i.

lowest value was 2.4 (for $R_e/R_i = 1.25$; $L/(2R_e) = 0.0625$; $R_a/R_i = 0.6$). For all values of R_e/R_i with values of $L/(2R_e) > 0.75$, and R_a/R_i nearest to 0.1, the *SCF* values are between 2.8 an d 3.2 showing a commune zone of inflection, that are also shown by other authors and suggest a relative low sensibility to the R_e/R_i, and $L/(2R_e)$ parameters for $R_a/R_i = 0.1$ values.

5. Fit model using dimensionless parameters

Once all the results of the simulation have been obtained, Fig. 13 shows the effect of the geometric relationships on the *SCF*. It is of great interest for the design of pressure vessels with large holes, to have an equation that allows to easily finding the value of *SCF* for a specific geometric configuration, based on the geometric relationships discussed in the previous sections. In this way, in order to obtain an adequate fit model, the authors initially analyze the sensitivity of *SCF* to R_a/R_i while keeping R_e/R_i and $L/(2R_e)$ fixed. Subsequently, only parameter $L/(2R_e)$ is kept fixed and it is observed how *SCF* varies as a function of R_e/R_i. According to these variations, the authors propose equation (6), which does not have a physical or theoretical meaning of the *SCF*, but of the effect of the geometric relationships (R_a/R_i and R_e/R_i) in *SCF* obtained from the simulations. The variables included in the model are limited to R_a/R_i and R_e/R_i for different values of $L/(2R_e)$, to limit the complexity and length of the model.

$$SCF = \zeta - \lambda \cdot e^{-\tau(R_a/R_i)} \cdot cos[\omega(R_a / R_i) + \varphi] \tag{6}$$

where;

$$\zeta = A + B \cdot sin[C \cdot (R_e / R_i) + D]$$

$$\lambda = E * cos[G \cdot (R_e / R_i) + H] + I$$

$$\tau = J + K \cdot (R_e / R_i)$$

$$\omega = L' \cdot e^{M(R_e/R_i)} \cdot cos[N \cdot (R_e / R_i) + O] + P$$

$$\varphi = Q \cdot e^{R \cdot \Psi} \cdot cos[S \cdot \Psi + T] + U$$

$$\Psi = R_e/R_i - 0.65$$

To this aim, the authors use the Statgraphics software, which allows statistical determination of the values of each of the constants (A to U) of equation (6), taking into account the evolution shown in Fig. 13. In this way, the global fit model presented in equation (6), predicts the stress concentrator factor (*SCF*) as a function of the size ratio (R_a/R_i), the thickness ratio (R_e/R_i) and applies to different aspect ratio ($L/(2R_e)$) by varying the constants from A to U (Table 4, Table 5 and Table 6).

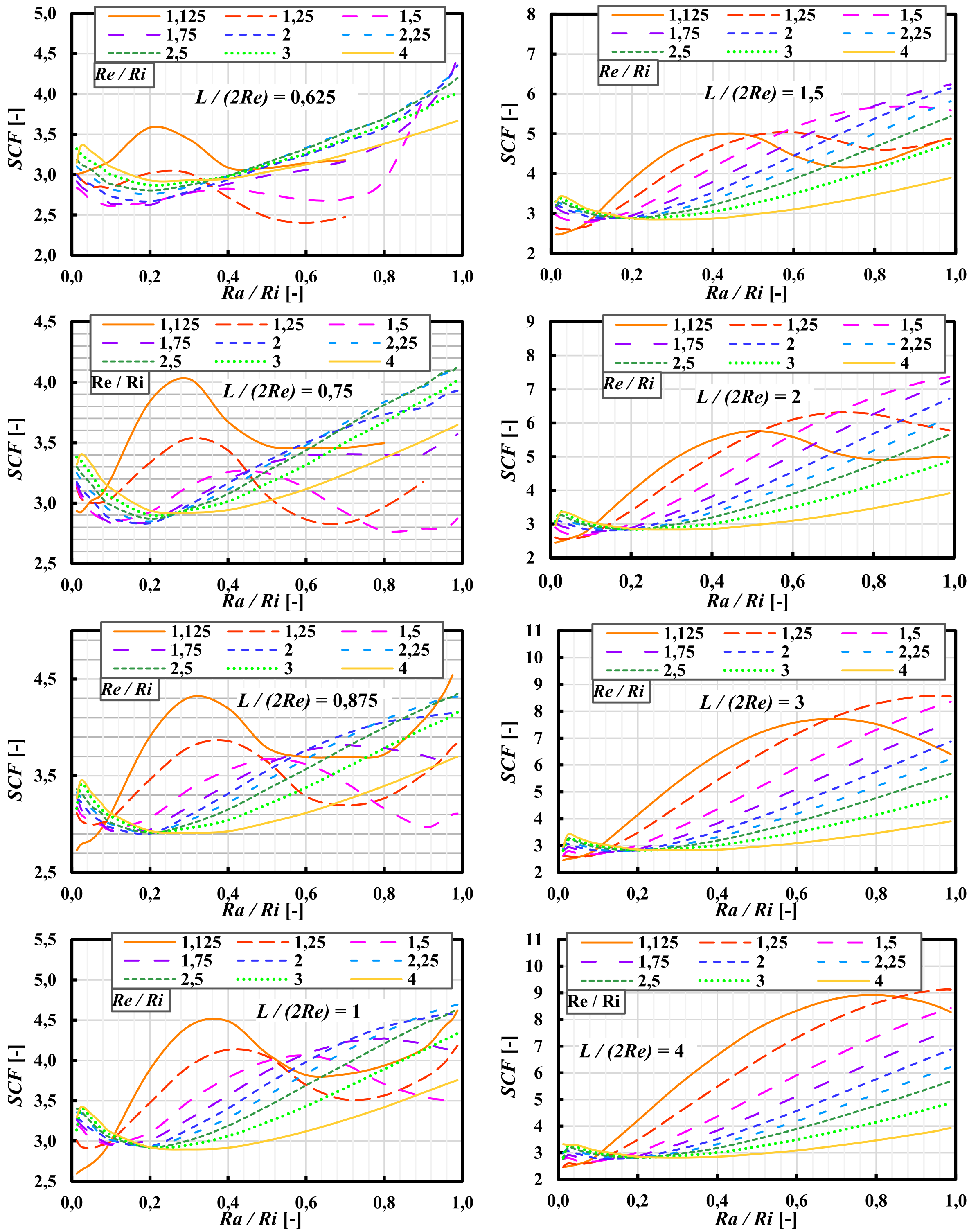

Fig. 13. Evolution of *SCF* for different values of R_e/R_i, R_a/R_i, and $L/(2R_e)$.

As an example, for $L/(2R_e) = 2$, Table 4 shows the estimated values for each constant (A to U) through the statistical study using the Marquardt estimation method (Statgraphics software), with a correlation coefficient R^2 of 99.08%, showing a good fit of the proposed model to the simulation data obtained. Table 4 shows the asymptotic error and the intervals (lower and upper) for a 95% confidence interval.

Fig. 14 shows the evolution of *SCF* obtained from the model (equation (6)) for an $L/(2R_e) = 2$ for different values of R_a/R_i and R_e/R_i. When comparing Fig. 14 (model) with Fig. 13 (for the same value of $L/(2R_e) = 2$), the good fit obtained statistically is evidenced, showing negligible differences when R_a/R_i approaches zero.

Similarly, the fit model (equation (6)) is applied for different values of $L/(2R_e)$ and for each of these the constants and the correlation coefficient (R^2) are obtained again as shown in Tables 5 and 6. The variable $L/(2R_e)$ has not been introduced in the correlation (equation (6)) in order not to be excessively complex.

The tabulated values in Tables 5 and 6, are useful in future studies to obtain an exact value of the *SCF* as a function of the dimensionless

Table 4
Statistically estimated constants for $L/(2R_e) = 2$.

	Estimate	Error	Lower	Upper
A	5.87243	0.0980817	5.67842	6.06645
B	2.35371	0.0561608	2.24262	2.4648
C	−107.97	1.23176	−110.407	−105.534
D	320.078	2.60091	314.933	325.222
E	−5.67637	0.139752	−5.95282	−5.39993
G	−116.331	0.660023	−117.636	−115.025
H	67.718	2.50167	62.7695	72.6666
I	5.3465	0.209388	4.93231	5.76069
J	3.61627	0.114802	3.38917	3.84336
K	−0.85885	0.0452558	−0.948371	−0.76933
L′	1976.53	278.557	1425.51	2527.55
M	−0.968788	0.0625958	−1.09261	−0.844967
N	−42.6847	2.27992	−47.1946	−38.1748
O	−388.765	3.5646	−395.816	−381.713
P	209.342	9.00266	191.534	227.15
Q	328.936	77.8571	174.926	482.945
R′	−2.13934	0.283113	−2.69937	−1.57931
S	34.0433	7.14803	19.9037	48.1828
T	−659.491	6.50134	−672.352	−646.631
U	−58.1806	1.58785	−61.3216	−55.0397

Table 5
Statistically estimated constants for $L/(2R_e) < 1$.

—	$L/(2R_e)$			
	0.625	0.750	0.875	1.000
A	5.17719	4.58489	4.82469	4.99127
B	2.35575	1.51165	1.39513	1.22057
C	−119.922	−114.529	−98.0588	−102.245
D	433.053	441.797	423.765	423.419
E	−3.59702	−2.35017	−2.01924	−2.01616
G	−123.512	−119.201	−104.127	−111.739
H	164.343	174.543	160.867	164.606
I	3.58965	2.44007	2.52638	3.04155
J	2.04636	3.18506	2.41475	3.35661
K	−0.44879	−0.794853	−0.519778	−0.774697
L′	4914.59	3773.13	2848.51	3204.92
M	−0.57629	−0.398451	−0.308604	−0.324903
N	−20.1416	−18.9695	−17.92	−16.1582
O	−426.597	−431.345	−434.216	−436.537
P	583.565	756.521	763.487	764.764
Q	3686.35	307.061	242.66	270.22
R′	−3.73822	−1.22322	−1.06648	−0.910646
S	36.1436	38.3746	33.9955	30.1892
T	−656.486	−657.797	−648.241	−643.339
U	−52.1502	−37.4654	−35.5196	−28.9093
R^2	86.6%	89.1%	92.9%	96.8%

parameters R_e/R_i, R_a/R_i and $L/(2R_e)$. Fig. 15 shows a contour map that allows to quickly locate and know the value of *SCF* for any value of R_e/R_i, R_a/R_i and $L/(2R_e)$ within the ranges established in this study (Table 2). In this way, values of $R_e/R_i \leq 2$ the *SCF* increases as $L/(2R_e)$ and R_a/R_i increase and for values of $R_e/R_i > 2$ the *SCF* is no longer dependent on the aspect ratio $L/(2R_e)$. In Fig. 15, the small dark areas (for R_e/R_i equals 1.125, 1.25 and 1.5), represent geometrically incompatible zones and therefore these combinations were not taken into account during the study.

Finally, comparing the simulation data (Fig. 13) with the fit model data (Fig. 15), a clear correspondence of the *SCF* values is observed, although the contour map allows us to observe the continuous behavior of the *SCF* when varying the dimensionless parameters R_a/R_i and $L/(2R_e)$ for each value of R_e/R_i. Thus, it is concluded that the *SCF* increases gradually as the cylinder aspect ratio increases and the hole size increases, for all values of R_e/R_i.

Table 6
Statistically estimated constants for $L/(2R_e) > 1$.

—	$L/(2R_e)$			
	1.5	2.0	3.0	4.0
A	5.07909	5.87243	5.89189	5.88183
B	1.53149	2.35371	2.20899	2.16963
C	−86.778	−107.97	−94.9887	−74.6168
D	300.428	320.078	268.044	210.921
E	−2.98539	−5.67637	−4.4904	−4.00222
G	−109.54	−116.331	−108.754	−96.8276
H	73.0618	67.718	42.4599	12.6292
I	4.00825	5.3465	5.26064	5.09826
J	4.29287	3.61627	2.1793	1.86163
K	−1.09777	−0.85885	−0.21861	−0.0734957
L′	2191.99	1976.53	618.216	68.1164
M	−0.506532	−0.968788	−1.10092	−0.200859
N	−17.6558	−42.6847	−94.2791	−110.085
O	−432.097	−388.765	−293.17	−256.044
P	374.406	209.342	136.559	135.763
Q	208.425	328.936	278.119	1026.96
R′	−1.85469	−2.13934	−3.19082	−4.15783
S	67.3123	34.0433	−0.405139	18.8221
T	−686.665	−659.491	−667.505	−664.201
U	−54.4126	−58.1806	−62.6983	−61.5961
R^2	98.6%	99.1%	99.0%	99.2%

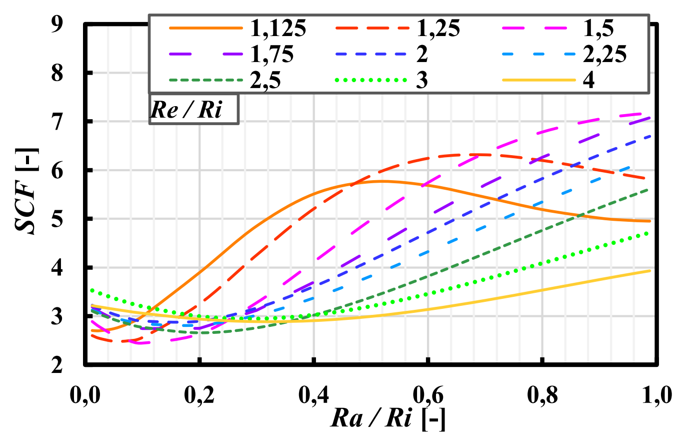

Fig. 14. *SCF* obtained from the model for $L/(2R_e) = 2$.

6. Conclusions

In this document, a three-dimensional finite element study was carried out to identify the maximum *SCF* and its location in pressure vessels with circular crossholes. This study was carried out using a wider range of geometric relationships used by other authors; this aspect enabled not only to compare the results of the present study with the particular results obtained by other authors but also to identify the behavior of the maximum *SCF* and its location in a wider range of geometric configurations (R_e/R_i between 1.125 and 4, R_a/R_i between 0.0125 and 0.9875, and $L/(2R_e)$ between 0.625 and 4).

From state of the art review, there is a lack of consistency in the methodology for the estimation of the *SCF* for a given geometry in pressurized vessel with orifices, no clear consensus among authors, finding at least four different ways to calculate it: $SCF_{\theta max}$, SCF_{1max}, $SCF_{\tau max}$, $SCF_{\sigma emax}$. In this study, initially a parametric validation of the mesh was carried out using the Lamé equation for cylinders without crosshole, finding a maximum average deviation of 8.5% for the smallest R_e/R_i thickness ratios. Subsequently, for the 1008 models of pressure vessel with crosshole, the maximum SCF 1max has been used and its

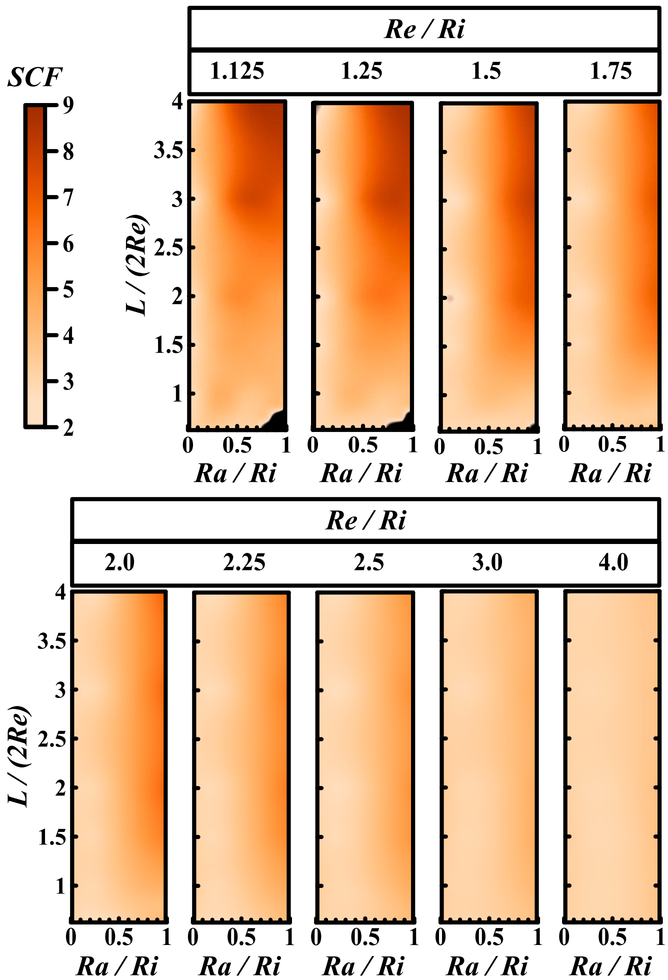

Fig. 15. Global evolution of the *SCF* obtained from the model.

respective location, establishing in this way three specific zones.

From the established zones, it was possible to identify that in most of the cases analyzed (approximately 60%) the maximum *SCF* is found in the corner G of the hole that corresponds to zone Z2 with values of $R_a/R_i = 0.3$. The other cases analyzed are distributed in zones Z1 and Z3. The Z1 zone corresponds to values of $R_a/R_i > 0.3$ and where the points of maximum *SCF* move away from point G up to 70% of the radius of the hole (edge G-J) as R_a/R_i increases. From that 70% it tends to move on the surface A for values of $R_a/R_i > 0.5$, reaching even in some cases up to the external wall of the cylinder. Regarding the Z3 zone for values of $R_a/R_i < 0.3$, the points of maximum *SCF* are located in an almost triangular area defined by the corner G, 40% of the radius of the hole (edge G-J) and 50% of the wall thickness (edge G-H).

In general, the influence of the aspect ratio, $L/(2R_e)$, both on the position and on the value of the maximum *SCF* was determined, finding that values below 2 have a high impact on the value of the maximum *SCF*, while values above 3 have no influence on said value. Regarding the location, although it depends on the other variables, small values of aspect ratio place the maximum stress point in zone Z2 (corner G) and high values of aspect ratio place the maximum *SCF* in zones Z1 or Z3, depending on the values of the other parameters.

Once the maximum *SCF* and its location have been determined, the information given here is useful for the design of cylindrical vessels with holes with different geometric configurations. In fact, from the present study it has been possible to show that always taking the location of the point of maximum stress in the corner G as a unique design criterion is not suitable, since the maximum value of *SCF* can move away from the corner G depending on the geometric configuration, according to the zones established in this study.

Finally, a fit model has been proposed, which is statistically representative of the data obtained from finite elements and allows determining the *SCF* as a function of R_a/R_i and R_e/R_i valid for different values of $L/(2R_e)$. Thus, the model defined in equation (6) is useful in the design of pressure vessels with hole, since it allows to obtain in a simple and fast way an accurate value of the maximum *SCF* by varying the dimensionless parameters. In addition, a contour map has been included, which allows to observe the behavior of the *SCF* continuously by varying R_a/R_i, $L/(2R_e)$ and R_e/R_i. Thus, globally for all the values of R_e/R_i, it is observed that the *SCF* gradually increases as the relationship between slenderness and hole size increases.

Declaration of competing interest

The authors declare that they have no known competing financial interests or personal relationships that could have appeared to influence the work reported in this paper.

Data availability

Data will be made available on request.

Acknowledgements

The researchers appreciate the support of the Colombian School of Engineering Julio Garavito in the development of the project.

References

[1] C.A. Adenya, J.M. Kihiu, Stress Concentration Factors in Thick Walled Cylinders with Elliptical Cross-Bores, 2010, pp. 181–200.
[2] D. Camilleri, D. Mackenzie, R. Hamilton, Shakedown of a thick cylinder with a radial crosshole, J. Pressure Vessel Technol. (2008) 131.
[3] T. Comlekci, D. Mackenzie, R. Hamilton, J. Wood, Elastic stress concentration at radial crossholes in pressurized thick cylinders, J. Strain Anal. Eng. Des. 42 (2007) 461–468.
[4] R.D. Dixon, D.T. Peters, J.G.M. Keltjens, Stress concentration factors of cross-bores in thick walled cylinders and blocks, J. Pressure Vessel Technol. 126 (2004) 184–187.
[5] R. Dixon, D. Peters, J. Keltjens, Stress Concentration Factors of Cross-Bores in Thick Walled Cylinders and Square Blocks, American Society of Mechanical Engineers, Pressure Vessels and Piping Division (Publication) PVP, 2002, p. 436.
[6] J.H. Faupel, D.B. Harris, Stress concentration in heavy-walled cylindrical pressure vessels - effect of elliptic and circular side holes, Ind. Eng. Chem. 49 (1957) 1979–1986.
[7] J.C. Gerdeen, Analysis of stress concentrations in thick cylinders with sideholes and crossholes, Journal of Engineering for Industry (1972) 815–824.
[8] T. Iwadate, H. Takeda, K. Chiba, J. Watanabe, Safety analysis at a cross-bore corner of high pressure reactors, J. High Pres. Inst. Jpn. 23 (1985) 245–253.
[9] A.R. Kharat, V. Kulkarni, Analysis of stress concentration at opening in pressure vessel using ANOVA, Int. J. Renew. Energy Technol. (2014) 261, 03.
[10] J.M. Kihiu, G.O. Rading, S.M. Mutuli, Overstraining of flush plain cross-bored cylinders, Proc. IME C J. Mech. Eng. Sci. 218 (2004) 143–153.
[11] J.M. Kihiu, G.O. Rading, S.M. Mutuli, Universal SCFs and optimal chamfering in cross-bored cylinders, Int. J. Pres. Ves. Pip. 84 (2007) 396–404.
[12] J. Kihiu, G. Rading, S. Mutuli, Geometric constants in plain cross-bored cylinders, Journal of Pressure Vessel Technology - Transactions of The Asme 125 (2003).
[13] S.K. Koh, Fatigue analysis of autofrettaged pressure vessels with radial holes, Int. J. Fatig. 22 (2000) 717–726.
[14] P. Makulsawatudom, D. Mackenzie, R. Hamilton, Stress concentration at crossholes in thick cylindrical vessels, J. Strain Anal. Eng. Des. 39 (2004) 471–481.
[15] L.M. Masu, Cross bore configuration and size effects on the stress distribution in thick-walled cylinders, Int. J. Pres. Ves. Pip. 72 (1997) 171–176.
[16] L. Mizzi, A. Spaggiari, Stress concentrations in skew pressurized holes: a numerical analysis, Int. J. Pres. Ves. Pip. 194 (2021), 104510.
[17] J.L.M. Morrison, B. Crossland, J.S.C. Parry, Fatigue strength of cylinders with cross-bores, J. Mech. Eng. Sci. 1 (1959) 207–210.

[18] K.B. Mulchandani, D.P. Shukla, Photoelastic investigation of stress intensifications in the interacting nozzle attachment region of pressure vessels, J. Strain Anal. Eng. Des. 30 (1995) 167–174.
[19] G.C. Nihous, C.K. Kinoshita, S.M. Masutani, Stress concentration factors for oblique holes in pressurized thick-walled cylinders, J. Pressure Vessel Technol. (2008) 130.
[20] P.K. Nziu, L.M. Masu, Cross bore size and wall thickness effects on elastic pressurised thick cylinders, Int. J. Mech. Mater. Eng. 14 (2019) 4.
[21] P.K. Nziu, L.M. Masu, Cross bore geometry configuration effects on stress concentration in high-pressure vessels: a review, Int. J. Mech. Mater. Eng. 14 (2019) 6.
[22] R. Payri, F.J. Salvador, J. Gimeno, O. Venegas, Study of cavitation phenomenon using different fuels in a transparent nozzle by hydraulic characterization and visualization, Exp. Therm. Fluid Sci. 44 (2013) 235–244.
[23] G. Raju, K.H. Babu, N.S. Nagaraju, K.K. Chand, Design and analysis of stress on thick walled cylinder with and with out holes, Int. Journal of Engineering Research and Applications 5 (2015) 75–83.
[24] S.P. Timoshenko, J.N. Goodier, Theory of Elasticity, second ed., McGraw-Hill Book Company, 1951.